Platinum Anions

Dibariumplatinide: $(Ba^{2+})_2Pt^{2-}\cdot 2e^-$ and Its Relation to the Alkaline-Earth-Metal Subnitrides**

*Andrey Karpov, Ulrich Wedig, Robert E. Dinnebier, and Martin Jansen**

Dedicated to Professor Arndt Simon on the occasion of his 65th birthday

Among the transition elements, gold and platinum are unique in that their first electron affinities are positive and of a magnitude comparable to those of typical non-metals. For instance, platinum with an electron affinity of 2.13 eV[1] even surpasses that of oxygen (1.46 eV),[1] while gold (2.31 eV)[1] approaches the value as determined for iodine (3.06 eV).[1] These experimental data are mirrored by calculations[2] demonstrating the 6s states of gold and platinum to experience the strongest relativistic stabilization and orbital contraction of all stable elements. The implications of these atomic properties for the chemistry of the respective elements have been addressed extensively,[3] while the number of observations adding experimental evidence is growing steadily. For gold, the large band gap of the long-known CsAu[4] has been attributed to relativistic effects. More recently, the intrinsic stability of the Au^- ion, for example, as a solvated anion in a liquid electrolyte[5] or as a particle diffusing through an insulating ionic solid,[6] has been demonstrated. Also, striking parallels to the chemistry of halogens have been uncovered, such as the close crystal chemical correspondences of auride and halide compounds,[7] and the disproportionation of elemental gold in basic media.[8] For platinum, only recently evidence for its capability to exist as an anion has been provided: Cs_2Pt,[9] forming red transparent crystals, shows full charge separation, and thus is composed of the ions Cs^+ and Pt^{2-}. Treating platinum with barium, which is less electropositive than cesium, again induces charge transfer, which now, however, is incomplete. Thus, in BaPt[10] platinum bears a charge of approximately −1 and, because of its open-shell character, forms infinite chains of homoatomic bonds. Offering more electrons by increasing the Ba/Pt ratio should render platinum less capable to forming Pt–Pt bonds. In agreement with this expectation, in the structures of Ca_3Pt_2[11] and Ba_3Pt_2[12] platinum pairs can be identified.[13] The bonds within the dumbbells, however, are weak and are easily expanded while adapting to the packing requirements. Extending this work, we now have managed to synthesize Ba_2Pt, a platinide with an even higher barium content, which indeed contains isolated platinide ions.

Ba_2Pt was synthesized from the elements, sealed in tantalum ampoules, at 1223 K in argon. The as obtained micro-crystalline samples (EDX: Ba/Pt = 2.1(2)) are shiny-black, sensitive to air and moisture. The melting point is at about 1100 K. The compound exhibits temperature independent diamagnetism ($\chi_{mol}(273\,K) = -75\times10^{-11}\,m^3mol^{-1}$). The electrical conductivity is of metallic character ($\rho(273\,K) = 0.17\,m\Omega\,cm$; $\rho(273\,K)/\rho(5\,K) = 1.37$). According to laboratory X-ray powder data the product is single phasic.[14] All reflections can be indexed assuming a trigonal crystal system, and the intensities are well reproduced by supposing the $CdCl_2$[15] type of structure. However, the *c/a* ratio corresponds to a cubic cell, within the limits of experimental error. To distinguish whether the $CdCl_2$ or the closely related cubic PrI_2-V[16] structure type is the correct one, we have recorded high-resolution synchrotron data (Figure 1). Subsequent Rietveld profile refinement clearly showed line splittings, and the trigonal $CdCl_2$ structure type being the correct one.[17]

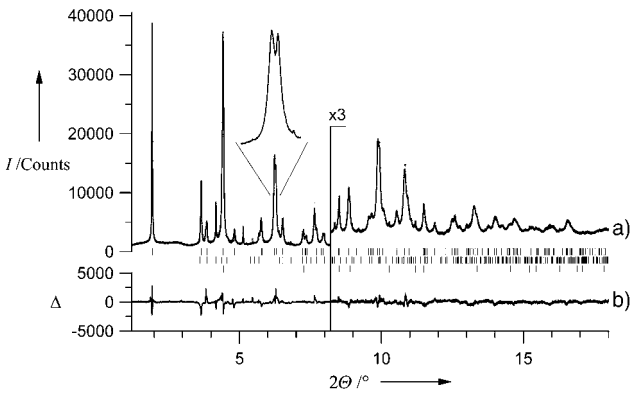

Figure 1. Scattered synchrotron X-ray intensity for Ba_2Pt as a function of diffraction angle 2Θ. Shown are the observed pattern (gray points), the best Rietveld-fit profile (line a), the difference curve between observed and calculated profile (line b), and the reflection markers (vertical bars: Ba_2Pt (top), BaH_2 (middle), and BaO (bottom)). The higher angle data starting at $2\Theta = 8.2°$ is enlarged by a factor of 3.

The resulting structure, is given in Figure 2. Ba_2Pt is the first example of a solid composed of two metals that adopts the $CdCl_2$ structure which is otherwise preferably found for ionic compounds with either a polarizable anion or cation. This strong indication for Ba_2Pt being a basically polar compound is corroborated by the observed bonding separations. Adding the effective radius of the Pt^{2-} ion, as derived[18] from Cs_2Pt[19] to the tabulated value for the Ba^{2+} ion[19] results in 303 pm which is in fair agreement with the observed Ba–Pt separation (315 pm). The distortion of the $PtBa_6$ octahedra (shrunk along one of the threefold axes) is due to the ratio $r(Pt^{2-})/r(Ba^{2+})$ of 1.04 which is not the ideal for an octahedral coordination (see Table 1). The interlayer Ba–Ba separations are enlarged in comparison to those in the elemental metal.

[*] Dipl.-Chem. A. Karpov, Dr. U. Wedig, Priv.-Doz. Dr. R. E. Dinnebier, Prof. Dr. M. Jansen
Max-Planck-Institut für Festkörperforschung
Heisenbergstrasse 1
70569 Stuttgart (Germany)
Fax: (+49) 711-689-1502
E-mail: m.jansen@fkf.mpg.de

[**] We thank Claus Muehle for his support of the experimental work, Roland Eger for hydrogen analysis, and the Fonds der Chemischen Industrie for continuous financial support. Special thanks to Andy Fitch (ESRF) for his help during synchrotron data collection.

 © 2005 Wiley-VCH Verlag GmbH & Co. KGaA, Weinheim DOI: 10.1002/ange.200462055

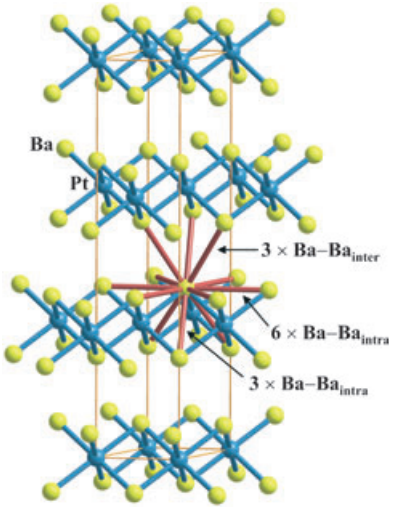

Figure 2. Perspective representation of the crystal structure of Ba_2Pt (blue spheres: platinum atoms; yellow spheres: barium atoms; orange lines: unit cell-edges).

These structural features justify the assignment of the charges as $(Ba^{2+})_2Pt^{2-}\cdot 2e^-$, in a first approximation.

From this scenario it is clear that Ba_2Pt has to be classified as another representative of the family of subvalent alkali and alkaline-earth compounds. This class of solids that has continued to arouse curiosity since the discovery of the first representatives,[20] is meanwhile well investigated,[21] and, furthermore, soundly based for structural and bonding concepts have been elaborated.[22] However, to date, one aspect appears not to be fully settled. The metal–metal separations in the interslab region are rather long, and moreover show variations from one compound to the other, which are hard to rationalize. One explanation, based on the low work function of these compounds and their characteristics as void metals, suggests Ba_2N, Ba_3N, and Cs_3O being expanded owing to the pressure of their conduction electron gases, in the metallic region.[23] Though providing just one more example, the features of Ba_2Pt are suited to shed some new light on this problem. To exclude ambiguities originating from different topologies, we restrict our considerations to $CdCl_2$ type representatives. Out of these, we disregard Tl_2O, Ag_2F, Ti_2O,and M_2C (M = rare-earth element) because of the totally different sets of valence orbitals available. The relevant structural data of the remaining alkaline-earth subnitrides, of Cs_2O and of Ba_2Pt are compiled in Table 1. The distortions of the octahedra, as expressed by the differences in the intraslab distances correlate with the deviations of their $r(X)/r(M)$ ratios from the value for an ideal octahedron (0.414), which lends support to regarding these parts of the structures constituted of the respective ions. Except for Cs_2O, in each case the interslab M–M separation $M–M_{inter}$ is significantly longer than in the pristine element M. The factors to be considered in trying to explain the trends are sizes of the cores M^{2+} and M^+, electrostatic M–M repulsion, metal-core polarizability, next-but-one-neighbor M–X Coulomb attraction, a reduction of the Coulomb interaction by the excess electrons in the interslab region, and the metallic bonding mediated by the excess electrons. These various interactions are of quite different effectiveness and thus have to be weighted, appropriately. Doubling the charge of M quadruples the interslab Coulomb repulsion. This would explain the conspicuously short interslab separations in Cs_2O. The increase of the interslab separation from calcium to barium can be partially attributed to the growing diameter of the M^{2+} cores, while the superproportional component to this increase might result from the diminishing M–X next-but-one-neighbor electrostatic attraction. The difference between Ba_2N and Ba_2Pt, finally, reflects the increase in metallic bonding in Ba_2Pt owing to the higher number valence electrons available.

To check the charge distribution suggested, particularly the role of platinum, and the relation of Ba_2Pt to the subnitrides, LMTO-TB-ASA band structure calculations[28] (LDA-functional,[29] relativistic partial waves) were performed for Ba_2Pt and Ba_2N. In both cases the polarization of the Ba core has been considered by including the 5p shell in the valence space, and the description of the interslab region has been improved by using nonstandard radii[30] of the atomic spheres. Owing to the polarization of the Ba core, the Ba 5p bands below −1 Ry are split significantly in Ba_2N. In Ba_2Pt such an extreme splitting is not observed (Figure 3), because of the softer anion. In this case dynamic correlation contributions have to be assumed.[9] Above −0.5 Ry, the densities of states of both Ba_2Pt and Ba_2N are very similar (Figure 3), showing a lower part describing the ionic layers and an upper delocalized part (Ba_2Pt: above −0.28 Ry; Ba_2N: above −0.19 Ry). The delocalized part is mainly built from

Table 1: Overview of selected crystallographic data and interatomic distances [ppm] of M_2X compounds crystallizing in the $CdCl_2$ structure type.

Compound	a	c/a	$(M–M_{intra})$; $(M–M)_{norm}$[a]	$(M–M_{intra})$; $(M–M)_{norm}$[a]	$(M–M_{inter})$; $(M–M)_{norm}$[a]	$(M–X)$; $(M–X)_{norm}$[b]	$r_{cryst}(X)/r_{cryst}(M)$
Cs_2O[24]	425.6(4)	4.46	383(2); 0.72	425.6(4); 0.80	419(2); 0.78	286(1); 0.93	0.70
Ca_2N[25]	361.58(5)	5.25	326.0(1); 0.83	361.6(1); 0.92	436.0(1); 1.10	243.4(1); 0.97	1.20
Sr_2N[25]	386.25(3)	5.36	351.4(2); 0.82	386.3(1); 0.90	473.9(1); 1.10	261.1(1); 0.97	1.04
Ba_2N[26]	401.7(3)	5.59	374.4(5); 0.84	401.7(3); 0.90	509.6(1); 1.15	274.6(3); 0.96	0.92
Ba_2Pt	456.42(1)	4.84	434.0(1); 0.98	456.4(1); 1.03	471.9(1); 1.06	314.9(1); 1.04[c] 0.87[d]	1.03

[a] $(M–M)_{norm} = (M–M)_{(M_2X)}/(2\times r_{met})$, where r_{met} are tabulated atomic radii in metals.[27] [b] $(M–X)_{norm} = (M–X)_{(M_2X)}/(r_{cryst}(M)+r_{cryst}(X))$; r_{cryst} are tabulated crystal radii for CN = 6,[19] except for N^{3-} where $r_{cryst}(CN=6)$ was estimated as $1.04\times r_{cryst}(CN=4)$.[27] [c] $(Ba–Pt)_{norm} = (Ba–Pt_{(Ba_2Pt)})/(r_{cryst}(Ba^{2+}{}_{CN=6}) + r_{cryst}(Pt^{2-}{}_{CN=6}))$; $r_{cryst}(Pt^{2-}{}_{CN=6}) = 154$ pm was derived[18] from Cs_2Pt (ECoN(Pt) = 6.5) [d] $(Ba–Pt)_{norm} = ((Ba–Pt)_{(Ba_2Pt)})/(r_{met}(Ba)+r_{met}(Pt))$. CN = coordination number, ECoN = effective coordination number.[18]

 © 2005 Wiley-VCH Verlag GmbH & Co. KGaA, Weinheim

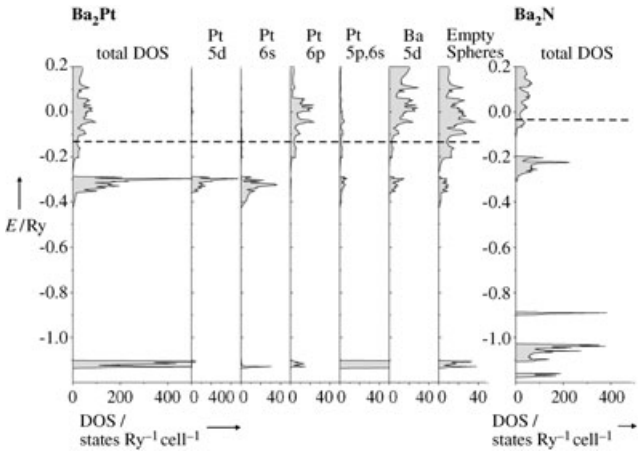

Figure 3. Total and partial densities of states (DOS; LMTO-TB-ASA) of Ba_2Pt (left). Total DOS of Ba_2N (right). The dashed line marks the Fermi level.

the orbitals of the empty spheres, which is also reflected by the electron distribution calculated for these bands (Figure 4). It should be noted that the electron density between the layers is very low. For this reason the domains of the electron localization function (ELF)[31] in the interslab region (Figure 4), which also are found in Sr_2N,[32] should be discussed cautiously. What can be stated from the ELF unambiguously is the ionic nature of the atoms, both in Ba_2Pt and Ba_2N, and the significant polarization of the ions. The ionicity of the layers is confirmed by COHP[33] calculations, which show in the valence region only a negligible antibonding contribution of +0.01 Ry for the Ba–Pt interaction.

The following partial charges are obtained from the topological analysis of the electron density according to Bader[34] in both, Ba_2Pt and Ba_2NPt: −1.8, N: −1.9, Ba: +0.9. The total electron density, however, does not contain any information on the local or delocalized character of any electrons. That is why with the Bader analysis the electrons in the interslab regions are added to the atomic basins, especially to those of Ba. From the integration of the DOS in the upper valence region (see above) we know that there are two delocalized electrons in Ba_2Pt and one delocalized electron in Ba_2N per formula unit, which must be subtracted from the partial charges. That is why the formal descriptions $(Ba^{2+})_2Pt^{2-}\cdot 2e^-$ and $(Ba^{2+})_2N^{3-}\cdot e^-$ are justified.

The larger volume of the Pt^{2-} ion compared to the N^{3-} ion (basin volumes from Bader analysis: 44.8 Å^3 (Pt) and 19.7 Å^3 (N)) is reflected only by a larger *a* parameter. The *c* parameter, and connected with this the interslab distance, in Ba_2Pt shrinks compared to Ba_2N, because the number of delocalized electrons in Ba_2Pt is doubled.

Ba_2Pt is another example for compounds containing platinum in a negative oxidation state with striking similarities to main-group elements. With increasing Ba/Pt ratio, going along from BaPt through Ba_3Pt_2 to Ba_2Pt, and thus with increasing number of valence electrons, the anionic subunits show decreasing covalent interaction, and are isolated ions in Ba_2Pt. In contrast to Cs_2Pt, the Ba compounds contain excess electrons, which are responsible for their metallic behavior.

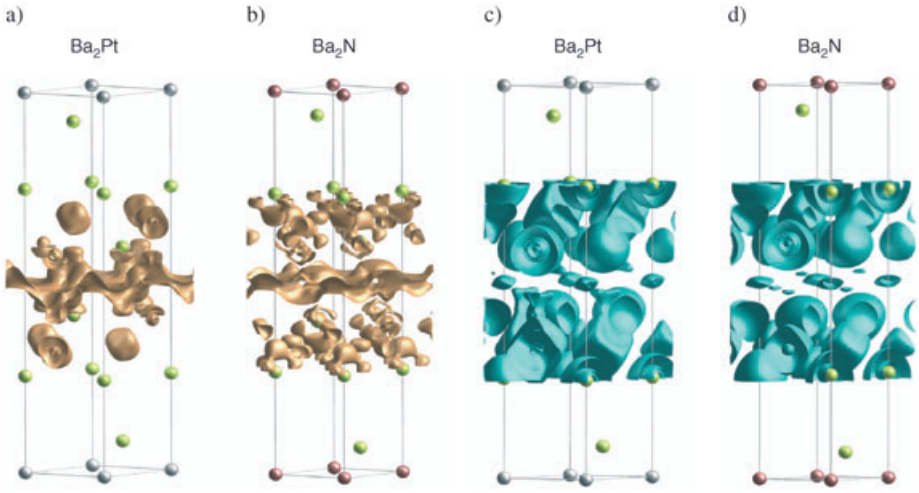

Figure 4. Electron densities computed from the highest occupied bands in a) Ba_2Pt ($\rho = 0.003\,e^-\,Bohr^{-3}$) and in b) Ba_2N ($\rho = 0.002\,e^-\,Bohr^{-3}$). Isosurfaces of the electron-localization function of c) Ba_2Pt and d) Ba_2N (both $\eta = 0.34$). Green spheres Ba, silver spheres Pt, purple spheres N.

Experimental Section

Ba_2Pt was prepared by reaction of barium (Sigma-Aldrich, 99.99%) with platinum sponge (MaTeck, 99.9%, dried and degassed before use at 673 K in the dynamic vacuum of 10^{-9} bar) in a 2.4:1 ratio. The mixture (≈0.5 g) was sealed under Ar in a tantalum tube, annealed at 1223 K for 2 days, and then cooled to room temperature with a rate of 10 K h^{-1}. The shiny-black product was isolated and handled under strictly inert conditions (Schlenk technique or glove box). Metal element analyses were performed using a scanning electron microscope (XL 30 TMP, Philips), equipped with an integrated energy dispersive X-ray (EDX) spectroscopy system. The hydrogen content was measured by oxidizing the sample mixed with V_2O_5 in an O_2 stream[35] and titration the evolved water pulse-coulometrically according to the Karl Fischer method.[36] Differential scanning calorimetry (DSC) was performed with a computer-controlled DSC sensor (DSC 404 C Pegasus, Netzsch). Temperature-dependent resistivity data was obtained for a pressed pellet connected to four probes of the resistivity measurement apparatus using the van der Pauw method[37] in the temperature range 5–290 K. Magnetization was measured using a SQUID magnetometer (MPMS 5.5, Quantum Design) in the temperature range 5–330 K at $H = 1$ T.

Received: September 21, 2004
Published online: December 21, 2004

Keywords: band structure calculation · barium · platinum · relativistic effects · structure elucidation

 © 2005 Wiley-VCH Verlag GmbH & Co. KGaA, Weinheim

[1] T. Andersen, H. K. Haugen, H. Hotop, *J. Phys. Chem. Ref. Data* **1999**, *28*, 1511 – 1533.
[2] J. P. Desclaux, *At. Data Nucl. Data Tables* **1973**, *12*, 311 – 406.
[3] P. Pyykkö, J. P. Desclaux, *Acc. Chem. Res.* **1979**, *12*, 276 – 281; P. Pyykkö, *Chem. Rev.* **1988**, *88*, 563 – 594.
[4] A. Sommer, *Nature* **1943**, *152*, 215; W. E. Spicer, A. H. Sommer, J. G. White, *Phys. Rev.* **1959**, *115*, 57 – 62.
[5] A.-V. Mudring, M. Jansen, J. Daniels, S. Krämer, M. Mehring, J. P. P. Ramalho, A. H. Romero, M. Parrinello, *Angew. Chem.* **2002**, *114*, 128 – 132; *Angew. Chem. Int. Ed.* **2002**, *41*, 120 – 124; P. D. C. Dietzel, M. Jansen, *Chem. Commun.* **2001**, 2208 – 2209.
[6] C. Feldmann, M. Jansen, *Angew. Chem.* **1993**, *105*, 1107 – 1108; *Angew. Chem. Int. Ed. Engl.* **1993**, *32*, 1049 – 1050; C. Feldmann, M. Jansen, *J. Chem. Soc. Chem. Commun.* **1994**, 1045 – 1046; A. Pantelouris, G. Küper, J. Hormes, C. Feldmann, M. Jansen, *J. Am. Chem. Soc.* **1995**, *117*, 11749 – 11753; C. Feldmann, M. Jansen, *Z. Anorg. Allg. Chem.* **1995**, *621*, 201 – 206.
[7] C. Feldmann, M. Jansen, *Z. Anorg. Allg. Chem.* **1995**, *621*, 1907 – 1912.
[8] A.-V. Mudring, M. Jansen, *Angew. Chem.* **2000**, *112*, 3194 – 3196; *Angew. Chem. Int. Ed.* **2000**, *39*, 3066 – 3067; A.-V. Mudring, J. Nuss, U. Wedig, M. Jansen, *J. Solid State Chem.* **2000**, *155*, 29 – 36.
[9] A. Karpov, J. Nuss, U. Wedig, M. Jansen, *Angew. Chem.* **2003**, *115*, 4966 – 4969; *Angew. Chem. Int. Ed.* **2003**, *42*, 4818 – 4821.
[10] A. Karpov, J. Nuss, U. Wedig, M. Jansen, *J. Am. Chem. Soc.* **2004**, *126*, 14123 – 14128.
[11] A. Palenzona, *J. Less-Common Met.* **1981**, *78*, P49-P53.
[12] A. Karpov, U. Wedig, M. Jansen, *Z. Naturforsch. B* **2004**, *59*, 1387 – 1394.
[13] In the system Ba–Pt two other alloys containing more platinum, $BaPt_2$ and $BaPt_5$, are also known.[38]
[14] The first samples synthesized were contaminated with small amounts of BaH_2 and BaO. Such a sample was used for the synchrotron experiment.[17] After barium metal was purified by heating in a closed Ta ampoule at 1173 K for 12 h in dynamic vacuum, followed by distillation at 1100 K, a hydrogen free product was obtained. The hydrogen analysis yielded 0.03(2) wt% of H, which is on the detection limit.
[15] L. Pauling, J. L. Hoard, *Z. Kristallogr.* **1930**, *74*, 546 – 551.
[16] E. Warkentin, H. Bärnighausen, *Z. Anorg. Allg. Chem.* **1979**, *459*, 187 – 200.
[17] Crystal structure data of Ba_2Pt: rhombohedral, space group $R\bar{3}m$ (No. 166), $a = 456.42(1)$, $c = 2209.12(5)$ pm, Pt in 3*a* (0,0,0), Ba in 6*c* (0,0,*z*) with $z = 0.25528(5)$, $V = 398.55(1) \times 10^6$ pm^3, $\rho_{calcd} = 5.872$ g cm^{-3}, $Z = 3$. Device for X-ray diffraction experiments: ID31 beamline at the European Synchrotron Radiation Facility (ESRF), Si(111) monochromator, 9-Ge(111) crystal analyzers, $\lambda = 24.804$ pm, 9 scintillation counters, $T = 298$ K, $1.0° < 2\Theta < 18.0°$ in steps of $0.002° 2\Theta$, glass capillary of 0.2 mm diameter. Structure determination process: Data reduction and background modelling by using the GUFI program,[39] three phases Rietveld refinement[40] using Ba_2N[26] as a starting model with barium hydride and barium oxide as impurity phases by using the GSAS program package,[41] $R_p = 0.053$, $R_{wp} = 0.072$, $R_F = 0.034$, $R_F^2 = 0.054$, number of reflections 131, number of variables 30. Further details on the crystal structure investigations may be obtained from the Fachinformationszentrum Karlsruhe, 76344 Eggenstein-Leopoldshafen, Germany (fax: (+49) 7247-808-666; e-mail: crysdata@fiz-karlsruhe.de), on quoting the depository number CSD-414463.
[18] R. Hoppe, *Z. Kristallogr.* **1979**, *150*, 23 – 52.
[19] R. D. Shannon, C. T. Prewitt, *Acta Crystallogr. Sect. B* **1969**, *25*, 925 – 946; R. D. Shannon, *Acta Crystallogr. Sect. A* **1976**, *32*, 751 – 767.
[20] E. Rengade, *C. R. Hebd. Seances Acad. Sci.* **1909**, *148*, 1199 – 1202.
[21] A. Simon, *Z. Anorg. Allg. Chem.* **1973**, *395*, 301 – 319; A. Simon, E. Westerbeck, *Z. Anorg. Allg. Chem.* **1977**, *428*, 187 – 198; A. Simon, *Z. Anorg. Allg. Chem.* **1977**, *431*, 5 – 16.
[22] A. Simon, *Struct. Bonding (Berlin)* **1979**, *36*, 81 – 127; A. Simon, *Coord. Chem. Rev.* **1997**, *163*, 253 – 270.
[23] U. Steinbrenner, A. Simon, *Z. Anorg. Allg. Chem.* **1998**, *624*, 228 – 232.
[24] K. R. Tsai, P. M. Harris, E. N. Lassettre, *J. Phys. Chem.* **1956**, *60*, 338 – 344.
[25] O. Reckeweg, F. J. DiSalvo, *Solid State Sci.* **2002**, *4*, 575 – 584.
[26] O. Seeger, Ph.D. Thesis, University of Tübingen, Germany, **1994**.
[27] U. Müller, *Anorganische Strukturchemie*, B. G. Teubner, Stuttgart, **1996**, pp. 46 – 50.
[28] R. W. Tank, O. Jepsen, A. Burkhardt, O. K. Andersen, TB-LMTO-ASA-Program, Version 4.7, Max-Planck-Institut für Festkörperforschung, Stuttgart, **1998**.
[29] U. von Barth, L. Hedin, *J. Phys. C* **1972**, *5*, 1629 – 1642.
[30] Radii of the muffin tin spheres (/Bohr) Ba_2Pt: Pt: 3.890, Ba: 3.025, E(0,0,1/2): 4.090, E1(0,0,3/8): 2.019, E2(0,0,1/8): 1.952; Ba_2N: N: 2.407, Ba: 3.612, E(0,0,1/2): 3.543, E1(0,0,1/8): 1.995.
[31] A. Savin, A. D. Becke, J. Flad, R. Nesper, H. Preuß, H. G. von Schnering, *Angew. Chem.* **1991**, *103*, 421 – 424; *Angew. Chem. Int. Ed. Engl.* **1991**, *30*, 409 – 412; A. Savin, O. Jepsen, J. Flad, O. K. Andersen, H. Preuß, H. G. von Schnering, *Angew. Chem.* **1992**, *104*, 186 – 188; *Angew. Chem. Int. Ed. Engl.* **1992**, *31*, 187 – 188.
[32] W. Bronger, R. Kniep, M. Kohout, *Z. Anorg. Allg. Chem.* **2004**, *630*, 117 – 121.
[33] R. Dronskowski, P. E. Blöchl, *J. Phys. Chem.* **1993**, *97*, 8617 – 8624.
[34] R. F. W. Bader, *Atoms in Molecules: a Quantum Theory*, Oxford University Press, Oxford, **1990**.
[35] R. Eger, H. Mattausch, A. Simon, *Z. Naturforsch. B* **1993**, *48*, 48 – 51.
[36] K. Fischer, *Angew. Chem.* **1935**, *48*, 394 – 396.
[37] L. J. van der Pauw, *Philips Res. Rep.* **1958**, *13*, 1 – 9; J. P. Suchet, *Electrical Conduction in Solid Materials* in *International Series of Monographs in the Science of the Solid State* (Gen. Ed.: B. R. Pamplin), Pergamon, Oxford, **1975**.
[38] H. Schulz, K. Ritapal, W. Bronger, W. Klemm, *Z. Anorg. Allg. Chem.* **1968**, *357*, 299 – 313.
[39] R. E. Dinnebier, GUFI a program for measurement and evaluation of powder pattern, Version 5.0, Heidelberger Geowiss. Abh. 68, Heidelberg, **1997**.
[40] H. M. Rietveld, *Acta Crystallogr.* **1967**, *23*, 151 – 152; H. M. Rietveld, *J. Appl. Crystallogr.* **1969**, *2*, 65 – 71.
[41] A. C. Larson, R. B. von Dreele, GSAS, General Structure Analysis System, Los Alamos National Laboratory Report LAUR 86 – 748, Los Alamos National Laboratory, Los Alamos, NM (USA), **2002**.

 © 2005 Wiley-VCH Verlag GmbH & Co. KGaA, Weinheim